AGU PUBLICATIONS

JGR

Journal of Geophysical Research: Atmospheres

RESEARCH ARTICLE
10.1002/2015JD023250

Key Points:
- NO_2 and HCHO from satellites can characterize O_3 production regimes and trends
- Transitional regime is dominated over eastern China in ozone season
- Cities in China are becoming increasingly VOC limited

Supporting Information:
- Figures S1–S3 and Tables S1 and S2

Correspondence to:
T. Holloway,
taholloway@wisc.edu

Citation:
Jin, X., and T. Holloway (2015), Spatial and temporal variability of ozone sensitivity over China observed from the Ozone Monitoring Instrument, *J. Geophys. Res. Atmos.*, *120*, 7229–7246, doi:10.1002/2015JD023250.

Received 11 FEB 2015
Accepted 27 MAY 2015
Accepted article online 29 MAY 2015
Published online 31 JUL 2015

Spatial and temporal variability of ozone sensitivity over China observed from the Ozone Monitoring Instrument

Xiaomeng Jin[1] and Tracey Holloway[1]

[1]Center for Sustainable and Global Environment, Nelson Institute of Environmental Studies, University of Wisconsin-Madison, Madison, Wisconsin, USA

Abstract Surface ozone (O_3) air pollution in populated regions has been attributed to emissions of nitrogen oxides ($NO + NO_2 = NO_x$) and reactive volatile organic compounds (VOCs). These constituents react with hydrogen oxide radicals ($OH + HO_2 = HO_x$) in the presence of sunlight and heat to produce O_3. The question of whether to reduce NO_x emissions, VOC emissions, or both is complicated by spatially and temporally heterogeneous ozone-NO_x-VOC sensitivity. This study characterizes spatial and temporal variations in O_3 sensitivity by analyzing the ratio of formaldehyde (HCHO, a marker of VOCs) to nitrogen dioxide (NO_2), a metric known as the formaldehyde nitrogen ratio (FNR). Level 3 gridded retrievals from the Ozone Monitoring Instrument (OMI) aboard the NASA Aura satellite were used to calculate FNR, with our analysis focusing on China. Based on previous studies, we take FNR < 1.0 as indicating VOC-limited regimes, FNR > 2.0 as indicating NO_x-limited regime, and FNR between 1.0 and 2.0 as indicating transitional regime (where either NO_x reductions or VOC reductions would be expected to reduce O_3). We find that the transitional regime is widespread over the North China Plain (NCP), the Yangtze River Delta, and the Pearl River Delta during the ozone season (defined as having near-surface air temperatures >20°C at the early afternoon OMI overpass time). Outside of these regions, the NO_x-limited regime is dominant. Because HCHO and NO_2 have distinct seasonal patterns, FNR also has a pronounced seasonality, consistent with the seasonal cycle of surface O_3. Examining trends from 2005 to 2013 indicates rapid growth in NO_2, especially over less-developed areas where O_3 photochemistry is NO_x limited. Over this time period, HCHO decreased in southern China, where VOC emissions are dominated by biogenic sources, but increased slightly over the NCP, where VOC emissions are dominated by anthropogenic sources. A linear regression approach suggests that most of China (70% of grid cells) will be characterized by a transitional regime during the O_3 season by 2030. However, in megacities such as Guangzhou, Shanghai, and Beijing, NO_2 has decreased such that the chemical regime has shifted from VOC limited in 2005 to transitional in 2013.

1. Introduction

It is well established that near-surface ozone (O_3) is harmful to human health, vegetation, and materials, especially at high concentrations [*Jacobson*, 2012]. Episodes of elevated O_3 pollution have been reported across China [*H. Wang et al.*, 2006; *T. Wang et al.*, 2006; *Chan and Yao*, 2008; *Shao et al.*, 2009; *Zhao et al.*, 2009; *Wang et al.*, 2011], where the 8 h average threshold for compliance with national regulations is 160 `μg/cm^3 (~80 ppbv) for most areas, including cities and croplands, and 100 μg/cm^3 (~50 ppbv) for national parks and protected regions (GB 3095-2012 (Ministry of Environmental Protection of China (2012), National Ambient Air Quality Standards, http://kjs.mep.gov.cn/hjbhbz/bzwb/dqhjbh/dqhjzlbz/201203/t20120302_224165.htm, accessed on 9 May 2015 (website in Chinese))). However, it was suggested that this level was not achieved on a regular basis, with nonattainment rates of 5.0–33.7% in the Beijing-Tianjin-Hebei region (part of the North China Plain, NCP), 2.2–27.1% in the Yangtze River Delta (YRD), and 5.5–15.5% in the Pearl River Delta (PRD) [*Liu et al.*, 2013a].

Ozone in near-surface, continental regions has been attributed to emissions of nitrogen oxides ($NO + NO_2 = NO_x$) and volatile organic compounds (VOCs), which react in the presence of hydroxyl (OH) and hydroperoxl (HO_2) radicals to create O_3. In China, emissions from power plants, industry, and transportation are the main contributor to NO_x emissions, accounting for more than 85% of the total NO_x release [*Zhao et al.*, 2013]. Emissions of VOCs may be anthropogenic, pyrogenic, or biogenic in origin. Most

biogenic VOCs (BVOCs) are more reactive than anthropogenic nonmethane VOCs (NMVOCs) and thus play a more significant role in O_3 formation [*Wei et al.*, 2007]. Other contributors to ground-level O_3 include long-range transport [*Jiang et al.*, 2010; *Nagashima et al.*, 2010] and stratosphere-troposphere exchange [*Wang et al.*, 2011]. As a result of industrial growth and expansion, the spatial extent of O_3 pollution is expanding and poses a risk to bothhuman health and agriculture [*Wang et al.*, 2005].

The effectiveness of emission controls depends on the photochemical regime of O_3 formation, namely, whether production is NO_x limited or VOC limited. In the VOC-limited (or NO_x-saturated) regime, VOC emission reductions reduce the chemical production of organic radicals (RO_2), which in turn lead to decreased cycling with NO_x and consequently lower concentration of O_3 [*Milford et al.*, 1989]. In the NO_x-limited (or VOC-saturated) regime, NO_x emission reductions reduce NO_2 photolysis, which is the primary source of free oxygen atoms, which react with O_2 to form O_3. So in a NO_x-limited regime, NO_x reductions reduce ambient O_3. In contrast, in the NO_x-saturated regime, NO_x acts to reduce ozone, so a decrease in emissions promotes O_3 production [*Kleinman*, 1994]. A transitional regime may also occur in which O_3 is sensitive to both NO_x and VOCs.

The O_3-NO_x-VOC sensitivity has been investigated through both models and observation-based methods. Modeling approaches offer explicit calculation of chemical sensitivities and complete data across chemical species, time, and space. However, results depend on emission inventories, meteorological inputs, chemical processes, and boundary layer dynamics [*J. Zhang et al.*, 2007], all of which have associated uncertainties. One model-based study from *Li et al.* [2013] found the O_3 responsiveness to NO_x emissions control in PRD to be spatially and temporally heterogeneous; another study from *Xing et al.* [2011] found the urban areas of Beijing, Shanghai, and Guangzhou to be VOC limited but the downwind rural areas to be NO_x limited. Observational analyses complement model-based studies by calculating O_3 sensitivity from ambient measurements. In situ observations of reactive NO_x, VOCs, and O_3 indicate that PRD was in VOC-limited regime in fall of 2004 [*Zhang et al.*, 2008]. Ozone sensitivity may also be derived from the measurements of secondary indicator species, such as reactive nitrogen (NO_y), which was used by *Chou et al.* [2009] to indicate that urban areas of Beijing were VOC limited in 2006. Due to resource constraints [*Zhang et al.*, 2008; *Kanaya et al.*, 2009], site measurements are often limited in time period and spatial extent.

Another indicator species for ozone regime is ratio of formaldehyde (HCHO) to NO_y [*Sillman*, 1995], which is particularly suited for analysis with satellite data. Space-based instruments have been used to evaluate temporal and spatial patterns in NO_x emissions [*Martin et al.*, 2003; *Q. Zhang et al.*, 2007] and VOC emissions [*Millet et al.*, 2006; *Barkley et al.*, 2013]. *Martin et al.* [2004] first applied the indicator ratio of *Sillman* [1995] to remotely sensed HCHO and NO_2 from the Global Ozone Monitoring Experiment (GOME) and proposed the formaldehyde to nitrogen dioxide ratio (FNR) as an indicator of O_3 sensitivity. *Choi et al.* [2012] found that GOME-based regime classification better captured the weekly cycle of O_3 than a model-based classification. The Ozone Monitoring Instrument (OMI) has finer spatial resolution than GOME, and *Duncan et al.* [2010] applied OMI data to characterize O_3 sensitivity over North America. This type of analysis was conducted over China by *Tang et al.* [2012], who used GOME data over the NCP (finding VOC-limited conditions in summer), and by *Witte et al.* [2009], who used OMI data over Beijing during the 2008 Olympic Games (and found sensitivity to both NO_x and VOCs).

This study represents the first large-scale and long-term characterization of O_3 sensitivity over China. We characterized the spatial and temporal trends of O_3-VOC-NO_x sensitivity over China from 2005 to 2013 using OMI satellite data, including an analysis of how space-based regime classification relates to sectoral emissions, meteorological conditions, and land cover.

2. Data and Methods

2.1. OMI Observation

The Ozone Monitoring Instrument (OMI) is a nadir-viewing spectrometer, launched on board the NASA Earth Observing Satellite Aura into Sun-synchronous orbit in July 2004. Since satellites in Sun-synchronous orbit keep pace with Earth's movement around the Sun, OMI passes the equator at constant local time (~13:45) everyday, providing daily global coverage. OMI covers two UV channels (264–311 nm and 307 – 383 nm)

and one visible light spectrometer channel (349–504 nm), with a spectral resolution between 0.42 and 0.63 nm and a spatial resolution of up to $13 \times 24\ km^2$. Comparing with the Global Ozone Monitoring Experiment (GOME) and SCanning Imaging Absorption spectroMeter for Atmospheric CHartographY (SCHIMACHY), OMI has finer spatial resolution, enabling better characterization of atmospheric chemistry from the space.

2.2. OMI NO_2 Column

We use the OMI operational standard NO_2 product, OMNO2 (version 2.1) [*Bucsela et al.*, 2013; *Lamsal et al.*, 2014], available from the NASA Goddard Earth Sciences and Data and Information Services Center (GES-DISC). The tropospheric NO_2 columns used in this study were calculated as follows: (1) retrieval of the slant column using a differential optical absorption spectroscopy (DOAS) technique in the 405–465 nm range [*Platt and Stutz*, 2008]; (2) calculation of stratospheric and tropospheric air mass factors (AMFs) by integrating the product of scattering weights and modeled NO_2 profile shape; (3) correction of "striping" effects along the orbital track; and (4) separation of tropospheric and stratospheric columns. Data version used in this study includes considerable improvements in the retrieval algorithm compared to previous version [*Bucsela et al.*, 2006; *Celarier et al.*, 2008]. Major improvements include finer-resolution radiative transfer calculation, monthly climatology of NO_2 profiles derived from a Global Modeling Initiative simulation, improved stripe correction, and improved stratosphere-troposphere separation (STS) scheme [*Bucsela et al.*, 2013].

The uncertainty of NO_2 column originates from errors in slant column retrieval, AMF calculation, and STS. Overall, *Bucsela et al.* [2013] estimate that the uncertainty in slant column retrieval is about 0.75×10^{15} molecules/cm^2; the uncertainty in stratospheric AMFs is small (~2%) and the uncertainty in tropospheric AMFs is 20% under clear-sky conditions; the error in STS algorithm is on the order of 0.2×10^{15} molecules/cm^2. The total uncertainty of OMI NO_2 column ranges from 30% to 60%, depending on the pollution level and cloud conditions [*Bucsela et al.*, 2013]. Evaluation of the product with a number of validation data sets indicates data accuracy within 20% [*Lamsal et al.*, 2014].

This study uses the Level 3 OMI NO_2 product (OMNO2D) available at $0.25° \times 0.25°$ grid. Level 3 data are weighted averages of good quality Level 2 OMINO2 pixel data that satisfy a screening criteria for clouds (cloud fraction $< 30\%$) and surface reflectivity (surface reflectivity < 0.3) [*Krotkov*, 2012]. The OMI data have been affected by row anomalies since May 2007; however, the cross-track scenes affected by row anomalies are filtered out in the Level 3 product.

2.3. OMI HCHO Column

Nine-year OMI HCHO daily products from 2005 to 2013 from the Belgian Institute for Space Aeronomy (Belgisch Instituut voor Ruimte-Aëronomie–Institut d'Aéronomie Spatiale de Belgique (BIRA-IASB)) were used in this study [*De Smedt et al.*, 2012]. Both the Smithsonian Astrophysical Observatory at Harvard University and the Belgian Institute for Space Aeronomy (BIRA-IASB) have recently made improvements on OMI HCHO products, which have addressed the instrumental degradation issues reported by previous studies [*Bucsela et al.*, 2013; *González Abad et al.*, 2015], thus allowing for better long-term monitoring of O_3 sensitivity from satellite data [*De Smedt et al.*, 2012]. Although some studies suggest striping effects and instrumental degradation in previous OMI HCHO products [*Witte et al.*, 2011], BIRA-IASB has made improvements to address these issues in the version 13 data. The instrumental degradation has been reduced by a factor of 2 through asymmetric Gaussian line-shape fitting during the irradiance calibration [*De Smedt et al.*, 2012], and row-dependent background normalization was applied to OMI products to reduce striping effects.

The retrieval of HCHO columns in the near-ultraviolet (UV) channels is based on differential optical absorption spectroscopy (DOAS) technique [*Platt and Stutz*, 2008]. First, the integrated column of trace gases along the optical path (termed the slant column) is estimated by fitting the measured reflectance with the HCHO absorption cross sections of *Meller and Moortgat* [2000] in the spectral range of 327.5–356.5 nm. The slant columns retrieved from operational algorithm are then converted to vertical columns by using air mass factors (AMFs). The profiles used for calculation of AMFs were obtained from the Intermediate Model for the Annual and Global Evolution of Species global chemistry-transport model [*Stavrakou et al.,* 2013]. The effects of aerosols were not explicitly considered in OMI HCHO retrievals but implicitly included in the

cloud correction, because effects of nonabsorbing aerosol and clouds on radiation are similar in the UV channels [*De Smedt et al.*, 2008]. For daily OMI BISA Level 3 products, pixels with lower than 40% cloud fraction were selected and averaged to $0.25° \times 0.25°$ grids. The cross-track scenes affected by row anomalies were filtered out in the Level 3 products.

The uncertainty sources of HCHO products include errors of slant column retrieval, errors on reference sector correction, and uncertainties associated with air mass factor estimation [*De Smedt et al.*, 2008]. The systematic errors with slant column of SCIAMACHY HCHO data range from 2 to 5×10^{15} molecules/cm^2 [*De Smedt et al.*, 2008]. The slant column error of OMI measurements is expected to be better than that for SCIAMACHY due to improved signal to noise [*Millet et al.*, 2008]. The errors on reference sector range from 5% to 25%, and errors on AMFs range from 10% to 25% in southeastern China [*De Smedt et al.*, 2012]. The total uncertainty of HCHO products ranges from 30% to 40% [*De Smedt et al.*, 2012].

2.4. O_3-NO_x-VOC Sensitivity Regime Classification

The ratio of HCHO/NO_2 functions as a reactivity-weighted VOC/NO_x ratio, since the production of HCHO is approximately proportional to the summed rate of reactions of VOC with peroxy radicals [*Sillman*, 1995]. HCHO is a short-lived oxidation product of many VOCs that may be measured with satellites; NO_x can be approximated from satellite observation of NO_2 column because of the short lifetime of NO_x and high ratio of NO_2/NO_x in the boundary layer [*Duncan et al.*, 2010].

Daily Level 3 OMI NO_2 and OMI HCHO data from 1 January 2005 to 31 December 2013 were used to calculate the O_3 indicator ratio. In order to reduce the random errors of satellite observation [*Millet et al.*, 2008; *Duncan et al.*, 2014], we first calculated 7 day average NO_2 and HCHO column. The O_3 indicator ratio, defined by the ratio of formaldehyde to nitrogen dioxide (FNR), was calculated based on the two 7 day averages. The combined uncertainty in FNR is 27–51% if the errors of OMI NO_2 and OMI HCHO are uncorrelated. However, as the effects of clouds, aerosol, and surface reflectivity on NO_2 and HCHO retrieval may be cancelled out, the uncertainty in FNR should be lower than the theoretical uncertainty [*Duncan et al.*, 2010].

Duncan et al.'s [2010] modeling study in Los Angeles suggests that FNR < 1.0 indicates VOC-limited regime, while FNR > 2.0 indicates NO_x-limited regime. However, different emission characteristics will likely affect the thresholds appropriate for determining O_3 sensitivity from indicator ratios [*Lu and Chang*, 1998]. Most urban areas in eastern China have similar VOC speciation and comparable O_3 pollution levels to Los Angeles [*Brown et al.*, 2007; *Song et al.*, 2007; *Wei et al.*, 2008; *Zheng et al.*, 2009], and the FNR thresholds from *Duncan et al.* [2010] have been used previously to investigate O_3-NO_x-VOC sensitivity in China [*Witte et al.*, 2011; *Tang et al.*, 2012]. Compared with Los Angeles, most cities in China have higher aerosol levels. Secondary aerosol production may become a large sink of radicals, which could shift O_3 production toward a VOC-limited regime under this definition [*Liu et al.*, 2012a].

It should be noted that temporal variation in FNR is not negligible see section 3.3.4, thus temporal averaging may offset the changes in O_3 sensitivity. Taking into account the temporal variation in FNR, we classified the regime based on the following criteria:

$FNR_{avg} < 1.0$ and $FNR_{avg} + FNR_{stddev} < 2.0$: VOC-limited Regime
$FNR_{avg} > 2.0$ and $FNR_{avg} - FNR_{stddev} > 1.0$: NO_x-limited Regime
Otherwise: Transitional Regime or Mixed Regime

In this definition, FNR_{avg} and FNR_{stddev} represent the temporal average and standard deviation of FNR. The term "transitional regime" refers to conditions whereby a reduction in either NO_x or VOC emissions could result in a reduction of ambient O_3; the term "mixed regime" refers conditions over spatial areas and time periods that include some combination of NO_x-limited, VOC-limited, and/or transitional regimes but where the specific regimes are not resolved in space and time.

Since the satellite retrievals we use exclude cloudiness, and OMI overpass time is in the afternoon, we assume that OMI data are retrieved on clear days with sunlight. Thus, variability in photolysis is not a major factor in our study results. However, temperature is also a major determinant of O_3 chemistry, and we separate results for warmer "ozone season" time periods and cooler "nonozone season" time periods. Because O_3 pollution

events are rare when the ambient temperature is below 20°C (68°F) [*Sillman*, 2003], we define the O_3 season as including all weeks where the 7 day average temperature at 1:00 P.M. local solar time > 20°C. This time period was selected to correspond with the satellite overpass time. Air temperature data were acquired from the National Centers for Environmental Prediction (NCEP) Climate Forecast System Reanalysis data set [*Saha et al.*, 2010]. The reanalysis 2 m temperature data are gridded at 0.5° × 0.5°. Monthly total precipitation data were obtained from Global Precipitation Climatology Center [*Schneider et al.*, 2013]. The spatial resolution is 0.5° × 0.5°.

2.5. Trend Detection

In this study, we applied a linear regression model as well as seasonal Kendall's test to detect and estimate the trend in satellite-derived HCHO, NO_2, and FNR. Multiple linear regression takes into account the seasonality of time series by means of periodic functions:

$$Y_t = \beta_0 + \beta_1 \cdot \sin\left(\frac{2\pi}{12}t\right) + \beta_2 \cdot \cos\left(\frac{2\pi}{12}t\right) + \beta_3 t + \varepsilon \tag{1}$$

where Y_t is the monthly NO_2, HCHO, or FNR of month t; β_0 is the monthly NO_2, HCHO, or FNR in January 2005; β_3 represents the linear trend in the time series, ε is the regression residual, which should be approximately normal; and β_1 and β_2 represent seasonal components of the time series, such that the amplitude of the annual cycle can be expressed as

$$A = \sqrt{\beta_1^2 + \beta_2^2} \tag{2}$$

The phase, which corresponds to the month with maximum NO_2, HCHO, or FNR is

$$t_{\max} = \frac{12}{2\pi}\tan^{-1}\left(\frac{\beta_1}{\beta_2}\right) \tag{3}$$

The linear model has been applied in previous studies [*van der A et al.*, 2006; *De Smedt et al.*, 2010], which is robust and has the advantage of characterizing seasonality. However, the linear regression model may be sensitive to data outliers. The seasonal Kendall's test [*Mann*, 1945] was used to complement the linear regression analysis. Kendall's test is nonparametric, which is less sensitive to data outliers, and calculated by considering the relationships (concordant and discordant) among data pairs [*Wilks*, 2011]. Seasonal Kendall's test takes into account the seasonality by computing the Kendall's test on each month and combining the results. Theil's method was used to estimate the magnitude of upward or downward trends in each month [*Sen*, 1968]. The annual trend was then computed as the median of the slopes in each month so that cross-season slopes can be avoided. A detailed description of the seasonal Kendall's test may be found in *Helsel and Hirsch* [1993].

2.6. Ancillary Data

2.6.1. MODIS Land Cover Data

We examine spatiotemporal patterns of photochemical regimes over different land cover types, so urban, cropland, and forest areas across China are taken from Level 3 annual Moderate Resolution Imaging Spectroradiometer (MODIS) land cover type product from 2005 to 2012 [*Friedl et al.*, 2010]. The MODIS product has finer spatial resolution at 500 m, which we resampled to 0.25° × 0.25° to match the OMI data. Grid cells that cover urban pixels were considered as urban. For the remaining pixels, we assigned the grid cell with cropland or forest if over 50% MODIS pixels belong to this land cover type. Otherwise the grid was classified as "other type."

2.6.2. Anthropogenic Emission Inventory

To relate the photochemical regimes with anthropogenic emissions, bottom-up NO_x and VOC emission data were obtained from the Multiresolution Emission Inventory for China (MEIC). MEIC was developed at Tsinghua University and provides gridded emission data for 2008 and 2010 [*Zhang et al.*, 2009; *Lei et al.*, 2011; *Li et al.*, 2014]. More than 800 anthropogenic sources were aggregated to four sectors, including residential use, transportation, power plants, and industry [*He*, 2012]. The MEIC emission inventory has been used in past studies [e.g., *Wang et al.*, 2014]; here monthly anthropogenic NO_x and VOC emission data at 0.25° resolution are used.

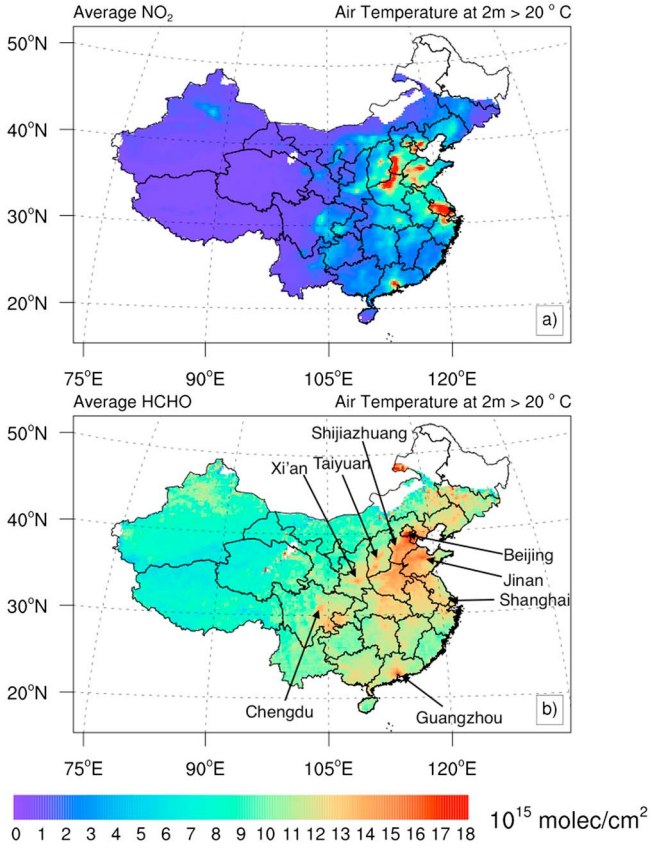

Figure 1. Nine year average of (a) HCHO and (b) NO_2 averaged from 2005 to 2013 in ozone season.

3. Results and Discussion

3.1. Variations of NO_2

3.1.1. Spatial Pattern

Figure 1a shows the average NO_2 column during the O_3 season, averaged over 2005–2013, as calculated from the 7 day composite of OMI data. The average NO_2 column over this period is 2.4×10^{15} molecules/cm^2, and the standard deviation is 8.9×10^{15} molecules/cm^2, indicating a highly dispersed spatial distribution of tropospheric NO_2. The tropospheric NO_2 column was higher in eastern China (>100°E) than western China (<100°E) by a factor of 5. Anthropogenic emissions are the main contributor to high NO_2 in East China, and the large gap between western and eastern China in population density and development level produced the large observed west-east difference in NO_2 column.

The NO_2 column over urban clusters, 7.6×10^{15} molecules/cm^2, is higher than the domain average NO_2 column by a factor of 3. Among the 30 capital cities (Harbin was excluded due to cold climate), tropospheric NO_2 column was higher than the upper fifth percentile (8.9×10^{15} molecules/cm^2) in 13 cities, and the highest 11 cities were all in the NCP, YRD, and PRD. The observed high-NO_2 column expands toward rural areas surrounding the urban clusters (Figure 1a). Areas in the top 5% of NO_2 column values consisted of 34% urban, 65% cropland, and 3% forest grid cells. The average NO_2 column over cropland was 6.6×10^{15} molecules/cm^2, which is close to the average over urban areas. High concentrations of NO_2 over rural areas are attributed to local emissions from heavy diesel vehicles on rural highways, agricultural burning, and the transport of NO_x from nearby cities [*Guoliang et al.*, 2008]. Over forested areas, the average NO_2 column was 2.4×10^{15} molecules/cm^2, 3 times lower than over urban areas.

3.1.2. Seasonal Variation

Figure 2b shows the time series of monthly average NO_2 column over the three industrial regions we discuss (NCP, YRD, and PRD). The maximum NO_2 column occurs in January, the minimum in July. Similar seasonality was found over other parts of China dominated by anthropogenic emissions. The winter peak in NO_2 is largely due to long lifetime of NO_x in these months as well as enhanced anthropogenic NO_x emissions due to the domestic heating [*Q. Zhang et al.*, 2007]. The average NO_2 in NCP reached 38.4×10^{15} molecules/cm^2 in January of 2012. However, *Q. Zhang et al.* [2007] noted that OMI NO_2 may overestimate wintertime NO_2 due to the impact of snow cover, zenith angle, and the wind speed. During the O_3 season of NCP (June to October on average), the regional average NO_2 column ranges from 5.9 to 16.1×10^{15} molecules/cm^2 and peaks in October (Figure 2a). YRD has longer O_3 season, which extends from March to December, and the regional average NO_2 column ranges from 3.7 to 19.7×10^{15} molecules/cm^2. An abrupt increase was observed from May to June over NCP and YRD from 2005 to 2012, which largely resulted from the emissions from agricultural residual burning following the winter wheat harvest [*Fu et al.*, 2007]. The abrupt increase disappeared in 2013, which may be attributed to emission controls on residual burning. In PRD, the average NO_2 column ranges from 3.1 to

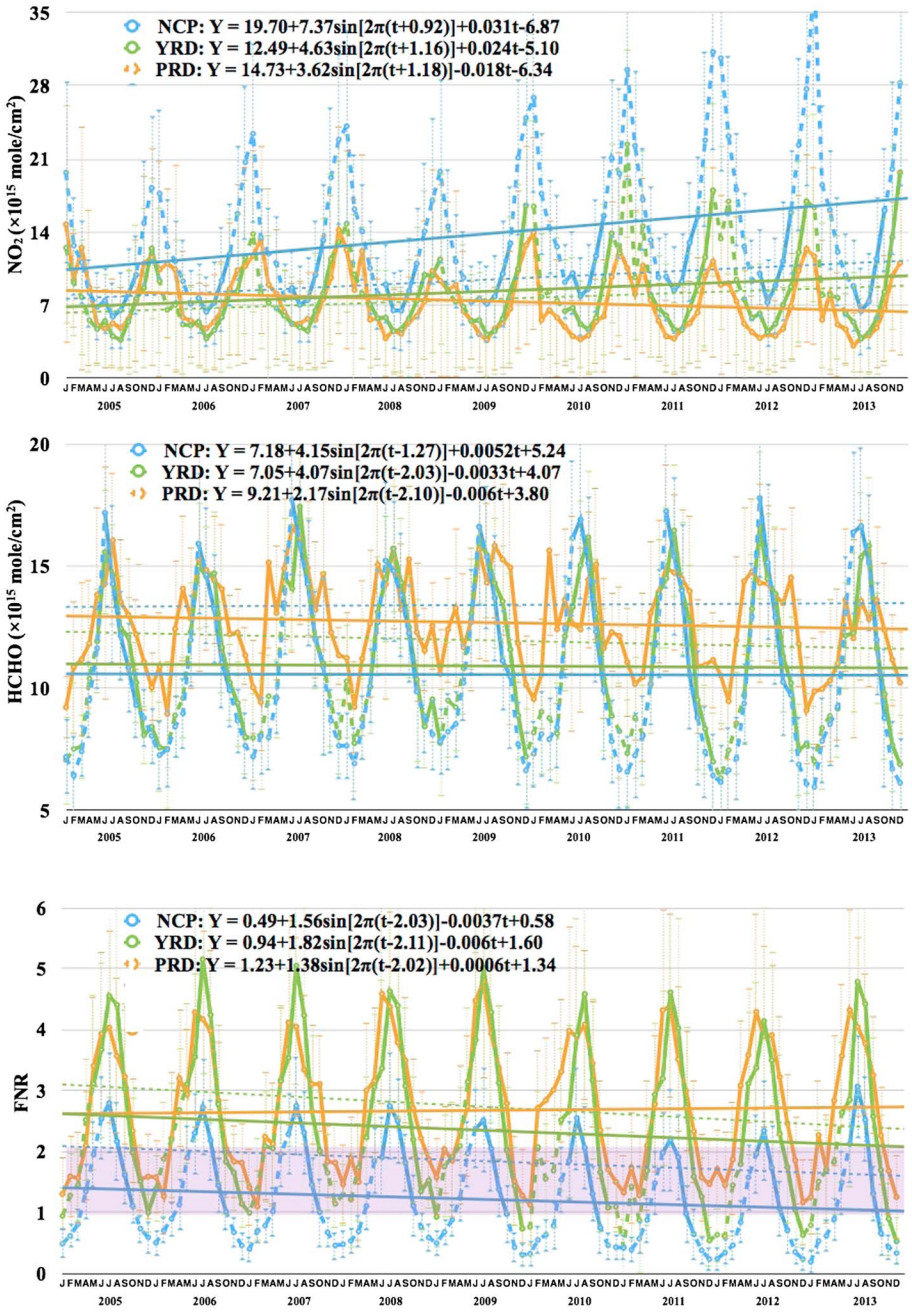

Figure 2. Time series of monthly average of (a) HCHO, (b) NO_2, and (c) FNR over urban areas of NCP, YRD, and PRD. The error bars represent the standard deviation. The dashed line indicates nonozone season, and the solid line indicates ozone season.

14.7×10^{15} molecules/cm^2. Since the average near-surface temperature is higher than 20°C throughout the year in PRD, the entire year is considered to be ozone season.

3.1.3. Interannual Trend

Both linear regression and Theil's method yield a statistically significant (>95%) increasing trend over most parts of China from 2005 to 2013 (Figure 3a and Figure S1 in the supporting information). The increasing trend is most pronounced in parts of the NCP, especially Shandong Province, southern Hebei Province, and northern Henan Province, where the tropospheric NO_2 column increased by more than 1×10^{15} molecules/cm^2 yr^{-1}. The regional annual trend was 0.4×10^{15} molecules cm^{-2} yr^{-1} in NCP and 0.29×10^{15} molecules/cm^2 yr^{-1} in YRD. Similar increasing trends have been reported in previous studies

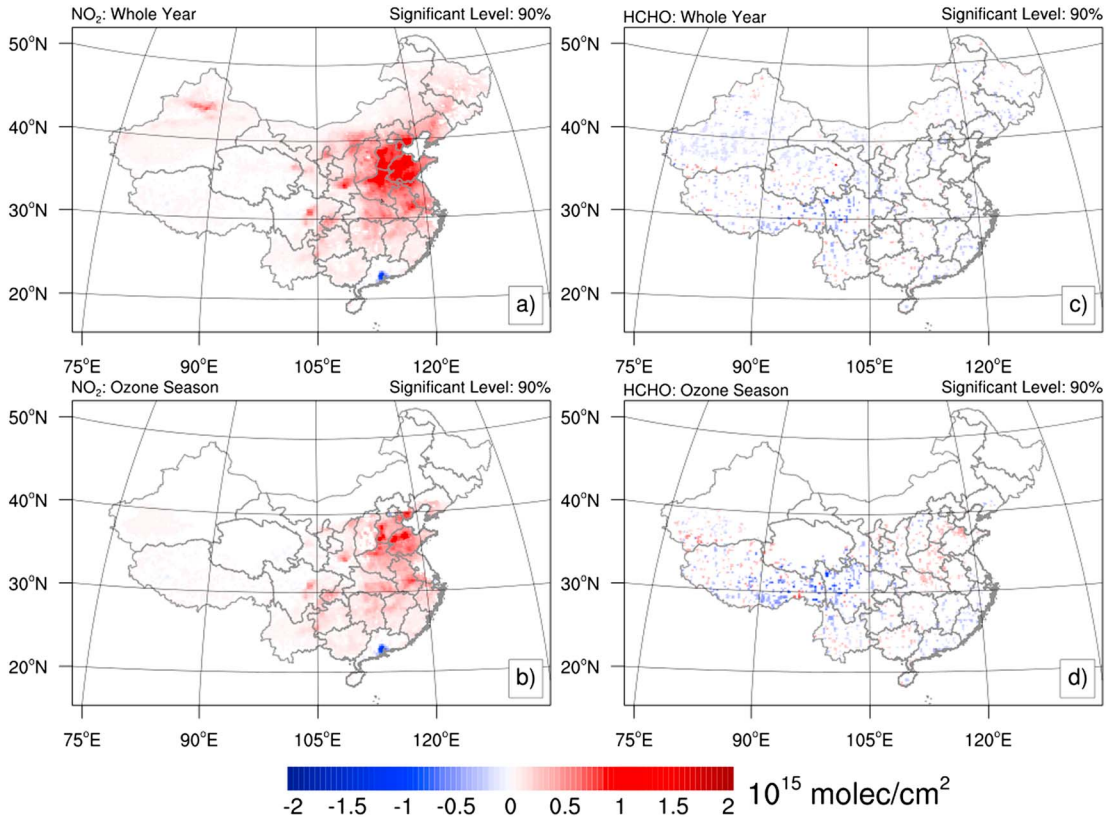

Figure 3. Linear trend from 2005 to 2013: (a) NO_2 in all seasons, (b) NO_2 in ozone season, (c) HCHO in all seasons, and (d) HCHO in ozone season.

[*Richter et al.*, 2005; *Q. Zhang et al.*, 2007; *Gu et al.*, 2013]. The increasing trend in NO_2 likely results from increasing anthropogenic NO_x emissions [*Richter et al.*, 2005]. As shown in Figure 2a, increasing trends are largely driven by the high-NO_2 column in winter; the increasing trend is slower during the O_3 season (Figure 3b). Relative to 2005, the growth rates in NO_2 were slower during the O_3 season across most parts of China, with the exception of northern Shandong Province.

Trend analysis over urban areas of the 31 capital cities of China indicates different trajectories between less developed capital cities and developed megacities (Table S1 in the supporting information). Linear regression identified statistically significant increasing trends in 25 out of the 31 capital cities and 17 out of 24 cities during the O_3 season. High growth rates were found in less developed inland cities, such as Xining, Urumqi, Yinchuan, Chengdu, and Xi'an. Even in terms of the magnitude of trend, the trends in these cities (0.40×10^{15} molecules/cm^2 yr^{-1} in Xining, 0.54×10^{15} molecules/cm^2 yr^{-1} in Urumqi, 0.58×10^{15} molecules/cm^2 yr^{-1} in Yinchuan, 0.64×10^{15} molecules/cm^2 yr^{-1} in Chengdu, 0.73×10^{15} molecules/cm^2 yr^{-1} in Xi'an) were higher than average (0.36×10^{15} molecules/cm^2 yr^{-1}). As we will discuss in section 3.3, the O_3 photochemistry in some of the cities is sensitive to NO_x emissions, suggesting that O_3 pollution is likely to worsen over the NO_x-limited cities as a result of increasing NO_2.

In contrast to most parts of China, insignificant or decreasing trends were found over economically developed megacities, including Beijing (−0.6%), Shanghai (−0.1%), and Guangzhou (−7.4%). The decreasing trend was more pronounced during the O_3 season with −2.5% in Beijing and −0.9% in Shanghai. Three factors may account for the decreasing NO_2 trends in megacities. First, vehicle emission controls are stricter, and enforcement is more effective in megacities than in other parts of China. In Guangzhou, 80% of buses and taxis have converted from gasoline engines to LPG engines, which has lower NO_x emission rates [*Gu et al.*, 2013]. Second, denitrification systems have been applied to thermal power plants in the vicinity of megacities in China, while the installation of denitrification systems has lagged in less developed cities. While the decreasing trend in NO_2 was insignificant over urban areas of Shanghai, a decreasing trend with 1.8% ($p < 0.01$) was found around the five power plants of Shanghai,

suggesting the effectiveness NO_x emission control from power plants. Finally, the international attention brought by the Olympics Games in Beijing in 2008, the World Expo in Shanghai in 2010, and the Asian Games in Guangzhou in 2010 provided additional incentives to improve air quality [*T. Wang et al.*, 2010; *Hao et al.*, 2011; *Liu et al.*, 2013b]. Due to the closure or relocation of heavy industries, the regional average NO_2 column in NCP decreased by 7% in 2008 (Figure 2a). Similar decreasing trends were also observed over YRD and PRD in 2010.

Trend detection using nonparametric Kendall's test yielded similar results to the linear regression. It is shown that Theil's method yielded higher growth rate when the NO_2 column was high and lower growth rate when the column was low. The linear regression trend is likely to be biased by extremes in winter at low NO_2 level and low extremes in summer at high NO_2 level. The trend of Theil's method is the median of slopes in each season, thus less likely to be biased by extreme values.

3.2. Variations of HCHO

3.2.1. Spatial Pattern

Figure 1b shows the 9 year average column density of HCHO during the (locally calculated) O_3 season. The average HCHO column density is 9.7×10^{15} molecules/cm^2 and the standard deviation is 4.5×10^{15} molecules/cm^2. The main HCHO source in the atmosphere is oxidation of methane (CH_4). Since CH_4 has a long lifetime, the HCHO column from CH_4 oxidation is relatively stable [*Millet et al.*, 2006], which is considered to be background level [*Boeke et al.*, 2011]. The spatiotemporal variation of HCHO is dominated by the oxidation of NMVOCs, including anthropogenic VOC [*Bo et al.*, 2008; *Zheng et al.*, 2009], biogenic VOCs from vegetation [*Wei et al.*, 2007], and pyrogenic emission from biomass burning [*Fu et al.*, 2007]. The average HCHO column is 53% higher in eastern China, where NMVOCs contribute to column abundance, than western China, where HCHO is mainly formed from CH_4 oxidation. Since biogenic VOC emissions are temperature dependent [*Duncan et al.*, 2009], higher HCHO column is expected in warmer areas such as southeast China. However, this temperature dependence is partially accounted for in Figure 1b because we only show composites above the 20°C temperature threshold. The spatial pattern of HCHO resembles that of NO_2 ($r = 0.68$), largely due to collocated anthropogenic NO_x and VOC emissions over populated regions.

The average HCHO column in urban areas (12.2×10^{15} molecules/cm^2) and cropland (12.4×10^{15} molecules/cm^2) is higher than forested areas (10.9×10^{15} molecules/cm^2). The difference between urban and cropland is generally insignificant. Biogenic VOC (BVOC) emissions contribute about 48% to the total reactive NMVOC in China [*Streets et al.*, 2003], and most BVOCs are more reactive than anthropogenic VOCs [*Wei et al.*, 2007], leading to the relatively high HCHO column over both croplands and forests. Despite the small difference in HCHO columns between urban areas and croplands, HCHO enhancement is observed in urban areas of some populated cities such as Beijing, Shijiazhuang, Taiyuan, Chengdu, Xi'an Shanghai, Jinan, and Guangzhou (marked in Figure 1b), where anthropogenic NMVOC emission overwhelms BVOC emissions.

3.2.2. Seasonal Variation

Figure 2b shows the time series of monthly average HCHO from 2005 to 2013 in the three heavily urban study regions. HCHO generally peaks in summer, the season favorable for O_3 formation. In NCP, maximum HCHO column is found in June and minimum is found in January. BVOC emission is exponentially correlated with temperature [*Duncan et al.*, 2009], and BVOC emission peaks in August in NCP [*Zhihui*, 2003]. The anthropogenic VOC emissions do not change much from June to August [*Zhang et al.*, 2009]. The maximum HCHO column in June is attributed to emission from biomass burning, especially agricultural burning over croplands [*Fu et al.*, 2007]. Biomass burning emissions led to higher HCHO level in croplands than urban areas in burning season. Over forests, the HCHO column in July approaches, and even exceeds, that in June. The seasonal cycle of HCHO in YRD resembles that in NCP, but HCHO column peaks later in June or early July due to more biogenic emission and less biomass burning emission compared with NCP [*Fu et al.*, 2007; *Stavrakou et al.*, 2014]. Due to the tropical climate, evergreen forest is dominated in PRD, which emits BVOCs throughout the year, leading to less significant seasonality of HCHO in PRD.

3.2.3. Interannual Trend

As HCHO is a short-lived oxidation product of many VOCs, the long-term trend in HCHO reflects the trend of reactive VOCs. The long-term trend in VOCs is of interest, especially over VOC-limited areas, where increases in VOC emissions may exacerbate O_3 pollution. As shown in Figures 3c and 3d, the detected increasing

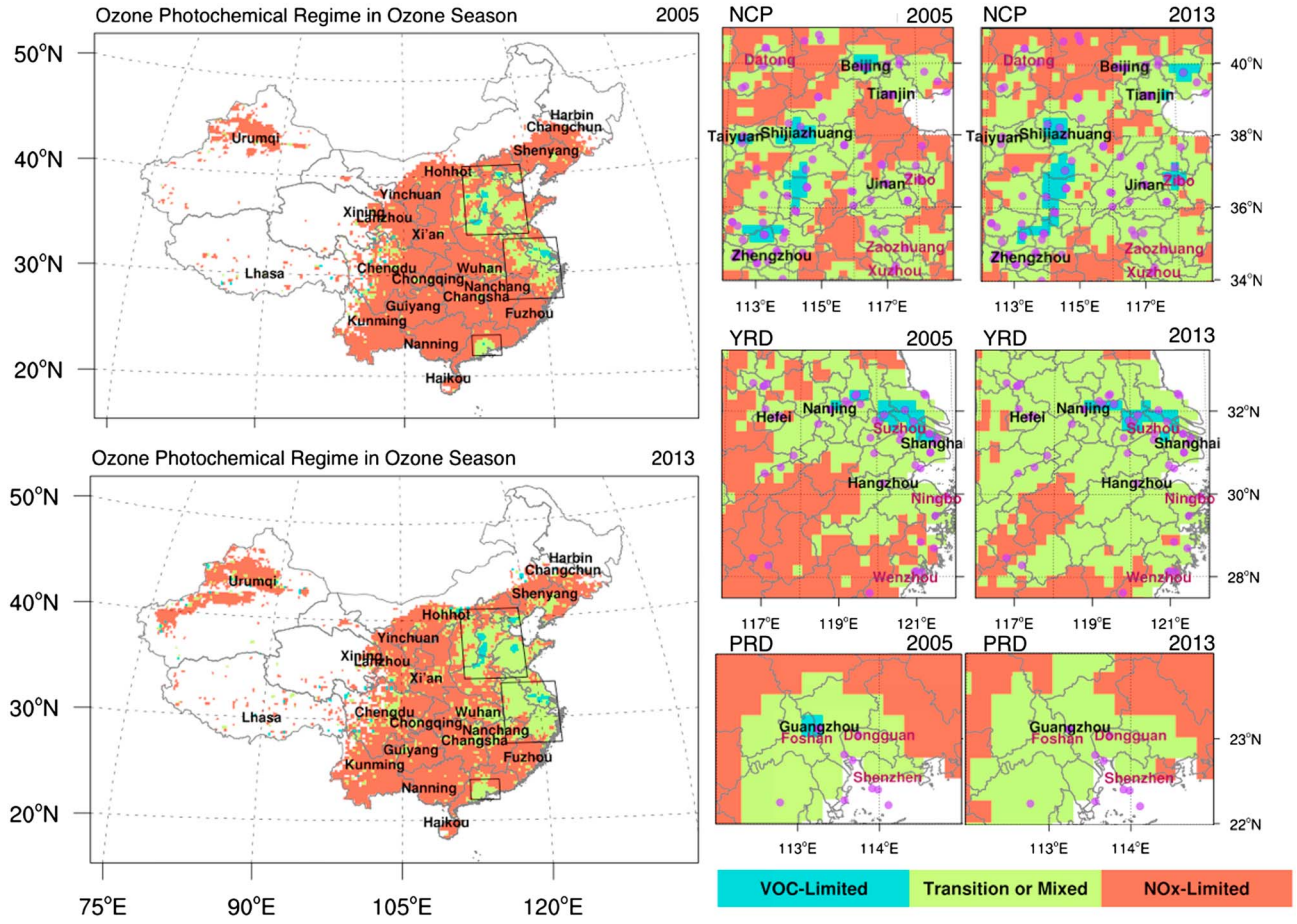

Figure 4. Photochemical regime classification in China and three subregions (North China Plain, Yangtze River Delta, and Pearl River Delta) in ozone season of 2005 and 2013. Cities marked in black are capitals of the first-level administrative regions. Cities marked in red are big cities with over 2 million population. The purple dots represent the locations of big power plants. The locations of ozone monitoring sites are marked with black dots.

or decreasing trends of HCHO were weak and insignificant in most parts of China. The regional annual trend is 0.6×10^{14} molecules $cm^{-2}\,yr^{-1}$ in NCP, -0.4×10^{14} molecules/$cm^2\,yr^{-1}$ in YRD, and -0.7×10^{14} molecules $cm^{-2}\,yr^{-1}$ in PRD. The magnitude of the increasing trend was slightly smaller than that observed from GOME and SCHIMACHY data ($0.8 \pm 0.2 \times 10^{14}$ molecules $cm^{-2}\,yr^{-1}$) [*De Smedt et al.*, 2010]. During the O_3 season, the increasing trend is dominant in central and northern China, while the decreasing trend is observed in western and southern China. In the NCP, the regional annual trend was observed over urban areas (0.6×10^{14} molecules $cm^{-2}\,yr^{-1}$) and croplands (1.4×10^{14} molecules $cm^{-2}\,yr^{-1}$), while a decreasing trend was observed over forests (-0.3×10^{14} molecules $cm^{-2}\,yr^{-1}$). In YRD and PRD, decreasing trends were found over all land cover types, with -0.5×10^{14} molecules $cm^{-2}\,yr^{-1}$ in YRD and -0.5×10^{14} molecules $cm^{-2}\,yr^{-1}$ in PRD. Anthropogenic NMVOC emissions have increased by 50% in China from 2000 to 2005 [*Bo et al.*, 2008], while BVOC emissions have decreased by 25% from 2007 to 2012 in China due to the impacts of climate and land use change [*Stavrakou et al.*, 2014]. The increasing anthropogenic emissions and decreasing BVOC emissions counteract to yield insignificant trend of HCHO from 2005 to 2013. In the O_3 season, the HCHO column increased slightly in urban areas and croplands of the NCP, where anthropogenic emissions overwhelm BVOC emission, but decreased in southern China, where BVOC emissions dominate HCHO production (Figure 3d).

3.3. O_3-NO_x-VOC Sensitivity

3.3.1. Spatial Variation

As a result of spatiotemporal heterogeneity of HCHO and NO_2, FNR varies in both space and time, as do the drivers of O_3 photochemistry across China. Figure 4 shows the photochemical regime classification over

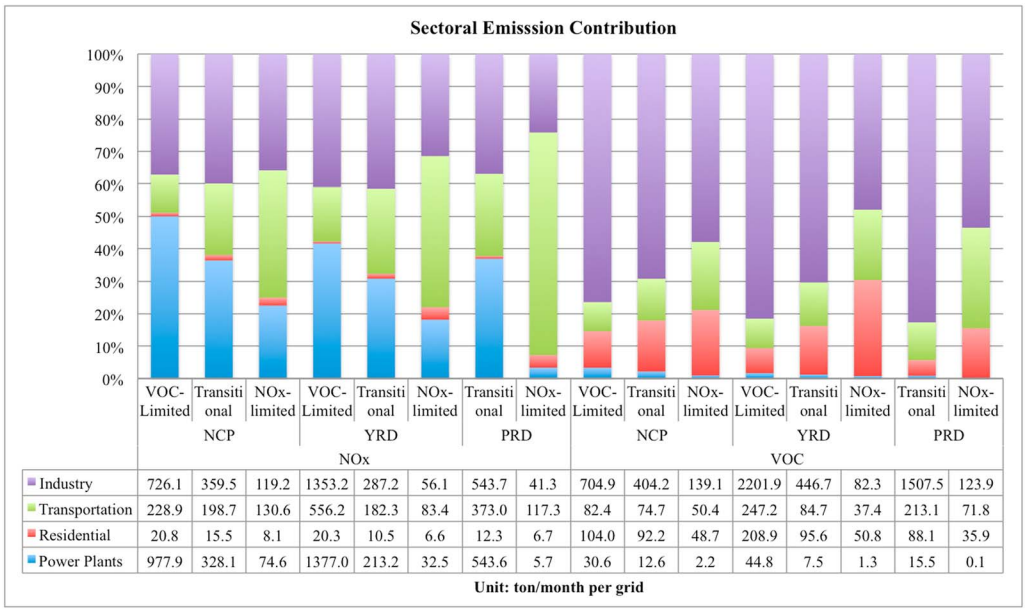

Figure 5. Anthropogenic NO_x and VOC emissions in VOC-limited, NO_x-limited, and transitional regimes. The upper bar chart shows the relative contribution of each sector to total NO_x or VOC emission. The bottom table shows the average emission from each sector.

China and over the three representative regions (NCP, YRD, and PRD) during the O_3 seasons of 2005 and 2013. A widespread transitional regime is observed over these regions, and NO_x-limited regime is dominant outside of these regions. In NCP, transitional or mixed regimes occupy 55% of the total grid cells in 2005 and 64% in 2013. A VOC-limited regime is found in central Beijing (2005), Tangshan (2013), Shijiazhuang (2005 and 2013), Zibo (2013), and some cities in Hebei Province with high density of power plants (Figure 3). Transitional or mixed regimes are found in downwind rural areas of Beijing (northern Beijing). In the YRD, a VOC-limited regime is found in southern Jiangsu Province and Shanghai (2005). Transitional or mixed regimes are dominant elsewhere, which occupy 47% of the total grid cells in 2005 and 78% in 2013. In PRD, VOC-limited regime is found in Guangzhou, and mixed or transitional regime was found over other populous cities (e.g., Shenzhen, Foshan, and Dongguan).

As shown in Figure 4, a VOC-limited regime is mostly found over the regions with high density of power plants, suggesting that the concentrated NO_x emission from power plants may lead to NO_x saturation and excessive consumption of OH. As expected in a VOC-limited regime, this excessive NO_x consequently mitigates the O_3 pollution, sometimes referred to as O_3 titration. Figure 5 shows the monthly average anthropogenic NO_x and VOC emissions from four sectors (industry, power plants, residential, and vehicles) and their contribution to each photochemical regime. The emissions inventory is collected for 2008, so regime classifications are based on 2008 satellite data analysis. Total anthropogenic VOC and NO_x emissions are highest in VOC-limited regimes and lowest in NO_x-limited regimes, as expected given that the VOC-limited regime is found over populated regions. Anthropogenic emissions are more scattered in NCP, leading to relatively less pronounced difference of among regimes.

In terms of sectors, point source NO_x emissions from power plants are concentrated in VOC-limited regimes (or transitional regimes in PRD), while vehicle NO_x emissions are distributed in all regimes. Power plants contribute most NO_x emissions in VOC-limited regime, industrial processes contribute most in transitional regime, and transportation contributes most in NO_x-limited regime. In rural areas where NO_x-limited regimes were found, heavy-duty diesel vehicles on rural highways emit huge amount of NO_x [*H. Wang et al.*, 2010]. As for anthropogenic VOC emissions, industry is the single largest source of anthropogenic VOC emission in all regimes, which contribute 50% to 80% of the total anthropogenic VOC emissions. In China, major sources of anthropogenic NMVOCs include solvent utilization, synthetic fiber, coke production, synthetic ammonia, and cement [*Bo et al.*, 2008]. Residential VOC emissions are the second

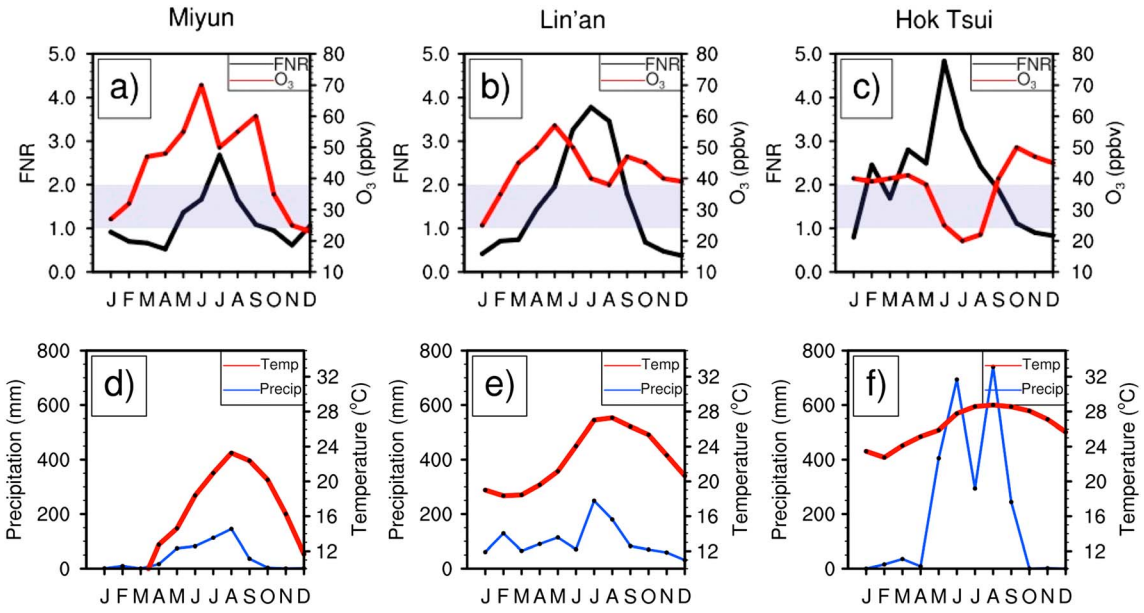

Figure 6. Monthly average O_3 concentration, FNR, near-surface air temperature, and precipitation in 2005 at (a and d) Miyun in NCP, (b and e) Linan in Yangtze River Delta, and (c and f) Hok Tsui in Pearl River Delta. The purple polygon represents the transition regime. The locations of ozone monitoring sites are marked with black dots.

largest source in NCP and in transitional and NO_x-limited regime in YRD. Vehicle emissions are a more important source than residential emissions in PRD. In addition to anthropogenic NMVOC, emissions from biogenic activities and biomass burning contribute about 50% and 6% to the total reactive NMVOC emissions in China [*Streets et al.*, 2003]. However, there are large discrepancies with BVOC and biomass burning emission inventory [*Fu et al.*, 2007; *Stavrakou et al.*, 2014], and a detailed analysis of BVOC and biomass burning is beyond the scope of this study.

3.3.2. Seasonal Variation

In addition to spatial heterogeneity, the FNR indicator ratio varies by season, day, and time of day in a given year. Figure 2c shows the time series of monthly regional average FNR over NCP, YRD, and PRD. The annual cycle is most pronounced in YRD ($A = 1.82$), covering two to three photochemical regimes every year. Since YRD has relatively warm climate, the O_3 season extends from spring to winter, and FNR ranges from 0.52 to 5.14. In NCP, the magnitude of seasonality is less pronounced ($A = 1.56$), and the annual cycle covers three regimes every year. During the O_3 season, monthly average FNR in the NCP covered transitional and NO_x-limited regimes before 2009, but since 2010, FNR in October has been VOC limited as a result of increasing NO_2 (section 3.1.3). In PRD, the O_3 photochemistry is NO_x limited from April to October and transitional or mixed in other months, implying that NO_x controls would be effective for O_3 reduction regardless of season.

Figure 6 shows the monthly average FNR along with O_3 concentrations reported in *Wang et al.* [2011], air temperature at 2 m, and precipitation in 2005 at three representative sites in three regions: (1) a rural site (Miyun) in the NCP (40°29′N, 116°46.45′E), (2) a rural site (Linan) in YRD (30°25′N, 119°46.44′E), and (3) a remote site (Hok Tsui, Hong Kong) in the PRD (22°13′N, 114°46.15′E). It is noteworthy that O_3 peaks were consistently observed in the month when O_3 sensitivity was in transition regime and about to shift to a NO_x-limited or a VOC-limited regime in the next month. That is, dual O_3 sensitivity is likely to cause O_3 enhancement. At the Miyun site (Figures 6a and 6d), peak O_3 was found in June, when O_3 photochemistry was in a transitional regime. Due to enhanced biomass burning emissions, concentrations of NO_x and VOC were high in June, contributing to enhanced O_3 pollution. High temperatures in June also accelerate the O_3 production rate [*Sillman and Samson*, 1995]. In July, the O_3 sensitivity shifted to NO_x-limited regime, and O_3 proceeded to decline due to lower concentration of NO_2 as well as increased precipitation (most likely indicating decreased daytime photolysis). In August and September, the O_3 photochemistry in Miyun site was transitional, and a second O_3 peak was observed in September, a warm month with relatively low precipitation. At the Linan site, surface O_3 peaked one month earlier (May) than Miyun site, which

Table 1. Comparison With Previous Studies

Period	Study Area	Ozone Sensitivity	FNR (This Study)	Method and Reference
July 2005	Beijing	urban: VOC limited rural: NOx limited	urban: 1.5 ± 0.6[a]; rural: 2.9 ± 1.1	community multiscale air quality model–response surface
	Shanghai		urban: 1.1 ± 0.4; rural: 2.1 ± 0.8	method [*Xing et al.*, 2011]
	Guangzhou		urban: 1.2 ± 0.5; rural: 2.3 ± 0.9	
Nov 2007	Guangzhou	VOC limited	0.6 ± 0.2	photochemical trajectory model
Aug 2007	Beijing			[*Cheng et al.*, 2010]
Summer 2006	Beijing	mixed photochemistry	1.25 ± 0.5	observation-based photochemical box model (OBM) [*Lu et al.*, 2010]
Aug–Sep 2006	Beijing urban area	VOC limited	0.9 ± 0.4	OBM [*Chou et al.*, 2009]
June – July 2005	Beijing	NOx limited or transitional	2.5 ± 1.0	Ground-based Measurements [*H. Wang et al.*, 2006; *T. Wang et al.*, 2006]
Nov 2006	PRD	mixed	1.7 ± 0.7 urban: 0.97 ± 0.4	chemical transport model (energy balance model) [*Li et al.*, 2013]
Summer 2009-2011	Miyun Site (Beijing)	VOC limited	1.8 ± 0.7	smog production algorithm (OBM) [*Wang et al.*, 2008]
Aug 2007	Beijing	transitional	1.25 ± 0.5	1-D photochemical model [*Liu et al.*, 2012a, 2012b]

[a]Assumes 40% uncertainty.

coincided with the last month with transitional regime in spring (Figures 6b and 6e). The O_3 sensitivity was in NO_x-limited regime throughout the summer, and relatively low O_3 level was observed, likely due to the summer peak in precipitation. In Hok Tsui site (Figures 6c and 6f), temperature is high throughout the year, which is favorable for O_3 formation, with concentrations at minimum during the summer months of heavy precipitation. O_3 enhancement in September and October coincided with dual O_3 sensitivity. O_3 pollution episodes in October in PRD have been documented in previous studies [*J. Zhang et al.*, 2007; *Li et al.*, 2013]. *Li et al.* [2013] indicated that peak O_3 is related to the formation of regime shift, consistent with our study results.

3.3.3. Comparison With Previous Studies

Several model and observation-based studies have investigated the O_3 sensitivity in China, with a focus on the three representative economic regions, shown in Table 1. Our findings are generally consistent with past work in identifying O_3 sensitivities over this region. Using a model-based analysis, *Xing et al.* [2011] found O_3 production sensitive to VOC emissions in urban areas of megacities in summertime, whereas we found that the largest cities are characterized by a transitional regime in the summer months. The discrepancy between these two studies, one based on a "bottom-up" model calculation and one based on a "top-down" satellite estimate, may be attributable to a wide range of factors. One possible explanation, based on *Fu et al.* [2007], is that the NMVOC inventory from *Streets et al.* [2003] used by *Xing et al.* [2011] underestimates anthropogenic and biomass burning VOC emissions by 25% and 80%, respectively. Our findings are consistent with *Lu et al.* [2010], who present an observation-based analysis finding mixed photochemistry in Beijing. It should also be noted that our study results are limited to early afternoon conditions and may not provide an "apples to apples" comparison with studies considering a 24 h period. O_3 formation is usually more VOC sensitive in the morning and becomes more NO_x sensitive as the NO_x consumed [*Sillman*, 1995]. The OMI overpass time tends to correspond with the daily NO_x minimum [*Chou et al.*, 2009; *Lu et al.*, 2010], which is also the most NO_x sensitive time of day. While once-a-day data is a limitation of OMI data analysis, ground level O_3 pollution often peaks in the afternoon [*Kanaya et al.*, 2009], so the O_3 sensitivity during this time of day should be of particular interest.

3.3.4. Interannual Trend

As a result of significant increasing trend in NO_2 but insignificant trend in HCHO, a widespread decreasing trend in FNR was found from 2005 to 2013. The decreasing trend in FNR led the O_3 photochemistry to become more sensitive to VOCs. As shown in Figure 4, the comparison between 2005 and 2013 indicates that the extent of VOC-limited regime does not expand significantly in O_3 season, but an expansion of transitional regime is observed over China. The percentage of VOC-limited regime in NCP during O_3 season has increased slightly from 4% to 6% in NCP, and transitional regime has increased from 55% to 64%. In YRD, VOC-limited regime has expanded from 3% to 4%, and the extent of transitional regime has increased from 47% to 78%. In PRD, the extent of transitional regime increased from 49% to 60%, but VOC-limited regime disappeared in 2013.

Similar expansion of transitional regime areas is also found outside the three regions, especially surrounding the capital cities, such as Wuhan, Changsha, Xian, Chengdu, and Chongqing.

Besides expanding spatial extent, we also find an extended transitional and VOC-limited regime during the ozone season. As shown in Figure 2, regional average FNR in NCP is VOC limited from November to March in 2005 and from September to April in 2012 and 2013. Over urban areas, O_3 formation has become sensitive to VOCs (VOC limited and transitional) throughout the year since 2007, except 2008 when Beijing Olympic Games were held. In YRD, O_3 sensitivity consistently has shifted from NO_x limited to transitional in October (from 2005 to 2013), but the spring shift from transitional back to NO_x limited has moved from April (prior to 2009) to May (since 2009).

In terms of regime shift over urban areas of the capital cities, 24 of the 31 capital cities show statistically significant decreasing trends in FNR (Table S2 in the supporting information, confidence level $>$ 95%). The number of capital cities with NO_x-limited photochemistry in urban areas during O_3 season is 20 in 2005 and decreased to 15 in 2013. Regime shift from NO_x-limited to transitional regime was observed over the cities with high growth rates of NO_2, such as Hohhot, Xi'an, Hefei, Chengdu, and Wuhan. Three cities, including Nanjing, Shijiazhuang, and Taiyuan shifted from transitional to VOC-limited regime (Figure 4). On the contrary, the most developed megacities, including Beijing, Shanghai, and Guangzhou, have shifted from VOC-limited regime in 2005 to transitional regime in 2013 as a result of decreasing NO_2. In 2005, O_3 production is NO_x saturated in these cities during O_3 season, so the titration effect of NO consumes O_3. As a result, the level of O_3 has increased in these cities despite significant efforts have been made to reduce NO_x emission. An O_3 pollution study in Beijing suggests that the daily average O_3 increased by 5% per year from 2005 to 2011, even though both reactive VOCs and NO_x emissions showed growth rates of -5% and -4% per year [*Zhang et al.*, 2014]. *T. Wang et al.* [2010] also found that the level of O_3 increased by 16% during the Olympic Games in 2008, although ambient concentration of NO_x dropped by 25%.

We consider the scenario of stable trends in FNR into the future across China. Under this scenario, the year when monthly average FNR reaches 1.0 or 2.0 can be predicted from equation (1). Such a trend suggests that China will move toward increasing sensitivity to VOC emissions, with most of the country characterized by a warm season transitional O_3 production regime by 2030 (70% of analyzed grid cells; Figure S2 in the supporting information). About 28% of NCP and 5% of YRD will become VOC limited by 2030. A VOC-limited regime is likely to occur throughout eastern China as early as 2025, but year-round VOC-limited photochemistry is unlikely to occur in the next four decades (Figure S3 in the supporting information). In the cities with transitional photochemistry, such as Hangzhou, Lanzhou, Nanjing, Tianjin, and Xi'an, VOC-limited regime will become dominant in the O_3 season by 2030 if the current trend continues. It should be noted that this linear extrapolation should not be viewed as a prediction given the rapidly changing landscape of energy and environmental policy in China. The Chinese government has formulated a series of policies to reduce emissions in 12th Five-Year-Plan (2010). Stronger enforcement and technology improvement is expected to slow down the increasing trend of NO_x emission, thus delaying the transition to VOC-limited regime. Model forecasts suggest that the growth rate of NO_x emissions from coal-fired power plants will slow down by at least 50% due to widespread application of emission control technologies [*Zhao et al.*, 2008].

4. Conclusion

This study applies satellite data to characterize O_3 sensitivity in China by calculating the ratio of HCHO to NO_2 from the OMI instrument aboard the Aura satellite. Satellites provide spatially continuous data, which could complement sparse in situ observations. We analyzed the spatial and temporal variation of NO_2, HCHO, and an O_3 sensitivity indicator (FNR) over China and in three heavily urban subregions. OMI observations suggest that O_3 sensitivity varies in both space and time and that O_3 production is more likely to be VOC limited over urban areas and NO_x limited over rural and remote areas. Both NO_2 and HCHO displayed distinct seasonality over China, resulting in variation of photochemical regimes with season.

The contribution of emission sectors to total NO_x and VOC emissions differs in different regimes: power plants contribute most NO_x in VOC-limited regime; industrial processes contribute most NO_x in transitional regime; and transportation contributes most NO_x to NO_x-limited regime.

A rapid growth in NO_2 was found in most parts of China through two complementary trend detection methods, especially western and central China where O_3 photochemistry is NO_x limited. Both parametric and nonparametric trend detection indicated insignificant trends in HCHO likely due to the net effect of increasing anthropogenic VOC emissions and decreasing biogenic VOC emissions. Rapid growth in NO_2 but insignificant trend in HCHO has caused the transition from NO_x limited to transitional or VOC-limited regimes in most parts of China. A linear regression model suggests that VOC-limited and transitional regimes would be dominant in the NCP region of China throughout the O_3 season by 2030 but that regime shift is unlikely to occur over southern China. In contrast, decreasing trends in NO_2 were found in developed megacities such Beijing, Shanghai, and Guangzhou, which may be attributed to stronger regulations and enforcement. The decreasing NO_2 trend has led to a regime shift from VOC-limited to transitional regime with high O_3 production efficiency and consequently increasing O_3 pollution.

Satellite data offers a powerful tool to inform O_3 chemistry and processes, and the benefits of this approach may be leveraged and strengthened through complementary analysis approaches. Modeling studies and field measurements will support evaluation of the FNR threshold criteria, especially the role of aerosol uptake of HO_2 and excess HONO [*Liu et al.*, 2012a]. And while primarily emitted HCHO only contributes to a small amount of the total HCHO, the separation of primarily emitted HCHO and secondary HCHO may allow a better approximation of the photochemical oxidation [*Garcia et al.*, 2006]. There are a number of model and observational strategies that could support the partitioning of primary and secondary HCHO. For example, satellite observations of glyoxal (CHOCHO) and CO have been shown to have the potential to separate emitted and photochemically produced HCHO. In addition, since CHOCHO is similarly formed from oxidation of most VOCs, with virtually no primary sources [*DiGangi et al.*, 2012], CHOCHO satellite products could also be directly used to characterize O_3 sensitivity [*Vrekoussis et al.*, 2010; *Huisman et al.*, 2011; *DiGangi et al.*, 2012; *Liu et al.*, 2012b]. Finally, satellite retrievals of trace gases represent a weighted average over all levels of the atmosphere contributing to the signal received by the space-based sensor [*Eskes and Boersma*, 2003]. The applicability of these vertical columns to ground level air quality is an emerging issue and complicated by conditions where vertical emission sources (e.g., NO_x from power plant smokestacks) interact with vertically heterogeneous chemical processes (e.g., NO titration effect caused by excessive NO_x aloft). Despite these limitations, space-based information offers a valuable resource for air quality management, energy planning, and public health assessment. By applying current generation satellite data to issues of policy relevance, new instruments and algorithms may be designed to strengthen and expand applications where space-based data prove most useful.

Acknowledgments

Support for this project was provided in part by the NASA Air Quality Applied Sciences Team (AQAST). We thank the National Atmospheric and Space Administration (NASA) for the free distribution of NO_2 data and MODIS land cover products; the Tropospheric Emission Monitoring Internet Service, part of the Data User Programme of the European Space Agency, for the free distribution of HCHO products; and the National Center for Environmental Protection (NCEP) for global reanalysis data. We acknowledge the free use of the Multiresolution Emission Inventory for China (MEIC) data (http://www.meicmodel.org), provided by Qiang Zhang. We also recognize the valuable assistance from colleagues at the University of Wisconsin-Madison Center for Sustainability and the Global Environment, including Monica Harkey and Xiujun Li, as well as AQAST collaborators Bryan Duncan and David Streets. We also thank very helpful comments from anonymous reviewers and Lok Lamsal.

References

Barkley, M. P., et al. (2013), Top-down isoprene emissions over tropical South America inferred from SCIAMACHY and OMI formaldehyde columns, *J. Geophys. Res. Atmos.*, *118*, 6849–6868, doi:10.1002/jgrd.50552.

Bo, Y., H. Cai, and S. D. Xie (2008), Spatial and temporal variation of historical anthropogenic NMVOCs emission inventories in China, *Atmos. Chem. Phys.*, *8*(23), 7297–7316, doi:10.5194/acp-8-7297-2008.

Boeke, N. L., et al. (2011), Formaldehyde columns from the Ozone Monitoring Instrument: Urban versus background levels and evaluation using aircraft data and a global model, *J. Geophys. Res.*, *116*, D05303, doi:10.1029/2010JD014870.

Brown, S. G., A. Frankel, and H. R. Hafner (2007), Source apportionment of VOCs in the Los Angeles area using positive matrix factorization, *Atmos. Environ.*, *41*(2), 227–237, doi:10.1016/j.atmosenv.2006.08.021.

Bucsela, E. J., E. A. Celarier, M. O. Wenig, J. F. Gleason, J. P. Veefkind, K. F. Boersma, and E. J. Brinksma (2006), Algorithm for NO_2 vertical column retrieval from the ozone monitoring instrument, *IEEE Trans. Geosci. Remote Sens.*, *44*(5), 1245–1258, doi:10.1109/TGRS.2005.863715.

Bucsela, E. J., N. A. Krotkov, E. A. Celarier, L. N. Lamsal, W. H. Swartz, P. K. Bhartia, K. F. Boersma, J. P. Veefkind, J. F. Gleason, and K. E. Pickering (2013), A new stratospheric and tropospheric NO_2 retrieval algorithm for nadir-viewing satellite instruments: Applications to OMI, *Atmos. Meas. Tech.*, *6*, 2607–2626, doi:10.5194/amt-6-2607-2013.

Celarier, E. A., et al. (2008), Validation of Ozone Monitoring Instrument nitrogen dioxide columns, *J. Geophys. Res.*, *113*, D15S15, doi:10.1029/2007JD008908.

Chan, C. K., and X. Yao (2008), Air pollution in megacities in China, *Atmos. Environ.*, *42*(1), 1–42, doi:10.1016/j.atmosenv.2007.09.003.

Cheng, H. R., H. Guo, S. M. Saunders, S. H. M. Lam, F. Jiang, X. M. Wang, I. J. Simpson, D. R. Blake, P. K. K. Louie, and T. J. Wang (2010), Assessing photochemical ozone formation in the Pearl River Delta with a photochemical trajectory model, *Atmos. Environ.*, *44*(34), 4199–4208, doi:10.1016/j.atmosenv.2010.07.019.

Choi, Y., H. Kim, D. Tong, and P. Lee (2012), Summertime weekly cycles of observed and modeled NO_x and O_3 concentrations as a function of satellite-derived ozone production sensitivity and land use types over the Continental United States, *Atmos. Chem. Phys.*, *12*(14), 6291–6307, doi:10.5194/acp-12-6291-2012.

Chou, C. C. K., C. Y. Tsai, C. J. Shiu, S. C. Liu, and T. Zhu (2009), Measurement of NO_y during campaign of air quality research in Beijing 2006 (CAREBeijing-2006): Implications for the ozone production efficiency of NO_x, *J. Geophys. Res.*, *114*, D00G01, doi:10.1029/2008JD010446.

De Smedt, I., J. F. Mueller, T. Stavrakou, R. van der A, H. Eskes, and M. Van Roozendael (2008), Twelve years of global observations of formaldehyde in the troposphere using GOME and SCIAMACHY sensors, *Atmos. Chem. Phys.*, *8*(16), 4947–4963.

De Smedt, I., T. Stavrakou, J. F. Müller, R. J. van der A, and M. Van Roozendael (2010), Trend detection in satellite observations of formaldehyde tropospheric columns, *Geophys. Res. Lett.*, *37*, L18808, doi:10.1029/2010GL044245.

De Smedt, I., M. Van Roozendael, T. Stavrakou, J. F. Müller, C. Lerot, N. Theys, P. Valks, N. Hao, and R. van der A (2012), Improved retrieval of global tropospheric formaldehyde columns from GOME-2/MetOp-A addressing noise reduction and instrumental degradation issues, *Atmos. Meas. Tech.*, *5*(11), 2933–2949, doi:10.5194/amt-5-2933-2012.

DiGangi, J. P., et al. (2012), Observations of glyoxal and formaldehyde as metrics for the anthropogenic impact on rural photochemistry, *Atmos. Chem. Phys.*, *12*(20), 9529–9543, doi:10.5194/acp-12-9529-2012.

Duncan, B. N., Y. Yoshida, M. R. Damon, A. R. Douglass, and J. C. Witte (2009), Temperature dependence of factors controlling isoprene emissions, *Geophys. Res. Lett.*, *36*, L05813, doi:10.1029/2008GL037090.

Duncan, B. N., et al. (2010), Application of OMI observations to a space-based indicator of NO_x and VOC controls on surface ozone formation, *Atmos. Environ.*, *44*, 2213–2223, doi:10.1016/j.atmosenv.2010.03.010.

Duncan, B. N., et al. (2014), Satellite data of atmospheric pollution for U.S. air quality applications: Examples of applications, summary of data end-user resources, answers to FAQs, and common mistakes to avoid, *Atmos. Environ.*, *94*, 647–662, doi:10.1016/j.atmosenv.2014.05.061.

Eskes, H. J., and K. F. Boersma (2003), Averaging kernels for DOAS total-column satellite retrievals, *Atmos. Chem. Phys.*, *3*(5), 1285–1291, doi:10.5194/acp-3-1285-2003.

Friedl, M. A., D. Sulla-Menashe, B. Tan, A. Schneider, N. Ramankutty, A. Sibley, and X. Huang (2010), MODIS Collection 5 global land cover: Algorithm refinements and characterization of new data sets, *Remote Sens. Environ.*, *114*(1), 168–182, doi:10.1016/j.rse.2009.08.016.

Fu, T.-M., D. J. Jacob, P. I. Palmer, K. Chance, Y. X. Wang, B. Barletta, D. R. Blake, J. C. Stanton, and M. J. Pilling (2007), Space-based formaldehyde measurements as constraints on volatile organic compound emissions in east and south Asia and implications for ozone, *J. Geophys. Res.*, *112*, D06312, doi:10.1029/2006JD007853.

Garcia, A. R., R. Volkamer, L. T. Molina, M. J. Molina, J. Samuelson, J. Mellqvist, B. Galle, S. C. Herndon, and C. E. Kolb (2006), Separation of emitted and photochemical formaldehyde in Mexico City using a statistical analysis and a new pair of gas-phase tracers, *Atmos. Chem. Phys.*, *6*, 4545–4557.

González Abad, G., X. Liu, K. Chance, H. Wang, T. P. Kurosu, and R. Suleiman (2015), Updated Smithsonian Astrophysical Observatory Ozone Monitoring Instrument (SAO OMI) formaldehyde retrieval, *Atmos. Meas. Tech.*, *8*(1), 19–32, doi:10.5194/amt-8-19-2015.

Gu, D., Y. Wang, C. Smeltzer, and Z. Liu (2013), Reduction in NO_x emission trends over China: Regional and seasonal variations, *Environ. Sci. Technol.*, *47*(22), 12,912–12,919, doi:10.1021/es401727e.

Guoliang, C., Z. Xiaoye, G. Sunling, and Z. Fangcheng (2008), Investigation on emission factors of particulate matter and gaseous pollutants from crop residue burning, *J. Environ. Sci.*, *20*(1), 50–55, doi:10.1016/S1001-0742(08)60007-8.

Hao, N., P. Valks, D. Loyola, Y. F. Cheng, and W. Zimmer (2011), Space-based measurements of air quality during the World Expo 2010 in Shanghai, *Environ. Res. Lett.*, *6*(4), 044004, doi:10.1088/1748-9326/6/4/044004.

He, K. (2012), Multiresolution Emission Inventory for China (MEIC): Model framework and 1990–2010 anthropogenic emissions, Abstract A32B-05 presented at 2012 Fall Meeting, AGU.

Helsel, D. R., and R. M. Hirsch (1993), *Statistical Methods in Water Resources*, Elsevier Science, New York.

Huisman, A. J., et al. (2011), Photochemical modeling of glyoxal at a rural site: Observations and analysis from BEARPEX 2007, *Atmos. Chem. Phys.*, *11*(17), 8883–8897, doi:10.5194/acp-11-8883-2011.

Jacobson, M. Z. (2012), *Air Pollution and Global Warming*, Cambridge Univ. Press, Cambridge, U. K.

Jiang, F., H. Guo, T. J. Wang, H. R. Cheng, X. M. Wang, I. J. Simpson, A. J. Ding, S. M. Saunders, S. H. M. Lam, and D. R. Blake (2010), An ozone episode in the Pearl River Delta: Field observation and model simulation, *J. Geophys. Res.*, *115*, D22305, doi:10.1029/2009JD013583.

Kanaya, Y., et al. (2009), Rates and regimes of photochemical ozone production over central East China in June 2006: A box model analysis using comprehensive measurements of ozone precursors, *Atmos. Chem. Phys.*, *9*(20), 7711–7723, doi:10.5194/acp-9-7711-2009.

Kleinman, L. I. (1994), Low and high No_x tropospheric photochemistry, *J. Geophys. Res.*, *99*, 16,831–16,838, doi:10.1029/94JD01028.

Krotkov, N. A. (2012), OMNO2 README File.

Lamsal, L. N., et al. (2014), Evaluation of OMI operational standard NO_2 column retrievals using in situ and surface-based NO_2 observations, *Atmos. Chem. Phys.*, *14*(21), 11,587–11,609, doi:10.5194/acp-14-11587-2014.

Lei, Y., Q. Zhang, K. B. He, and D. G. Streets (2011), Primary anthropogenic aerosol emission trends for China, 1990–2005, *Atmos. Chem. Phys.*, *11*(3), 931–954, doi:10.5194/acp-11-931-2011.

Li, M., et al. (2014), Mapping Asian anthropogenic emissions of nonmethane volatile organic compounds to multiple chemical mechanisms, *Atmos. Chem. Phys.*, *14*(11), 5617–5638, doi:10.5194/acp-14-5617-2014.

Li, Y., A. K. H. Lau, J. C. H. Fung, J. Zheng, and S. Liu (2013), Importance of NO_x control for peak ozone reduction in the Pearl River Delta region, *J. Geophys. Res. Atmos.*, *118*, 9428–9443, doi:10.1002/jgrd.50659.

Liu, H., X. M. Wang, J. M. Pang, and K. B. He (2013a), Feasibility and difficulties of China's new air quality standard compliance: PRD case of $PM_{2.5}$ and ozone from 2010 to 2025, *Atmos. Chem. Phys.*, *13*(23), 12,013–12,027, doi:10.5194/acp-13-12013-2013.

Liu, H., X. Wang, J. Zhang, K. He, Y. Wu, and J. Xu (2013b), Emission controls and changes in air quality in Guangzhou during the Asian Games, *Atmos. Environ.*, *76*, 81–93, doi:10.1016/j.atmosenv.2012.08.004.

Liu, Z., et al. (2012a), Summertime photochemistry during CAREBeijing-2007: RO_x budgets and O_3 formation, *Atmos. Chem. Phys.*, *12*(16), 7737–7752, doi:10.5194/acp-12-7737-2012.

Liu, Z., et al. (2012b), Exploring the missing source of glyoxal (CHOCHO) over China, *Geophys. Res. Lett.*, *39*, L10812, doi:10.1029/2012GL051645.

Lu, C. H., and J. S. Chang (1998), On the indicator-based approach to assess ozone sensitivities and emissions features, *J. Geophys. Res.*, *103*, 3453–3462, doi:10.1029/97JD03128.

Lu, K., et al. (2010), Oxidant (O-3+NO_2) production processes and formation regimes in Beijing, *J. Geophys. Res.*, *115*, D10306, doi:10.1029/2010JD014394.

Mann, H. B. (1945), Nonparametric tests against trend, *Econometrica*, *13*(3), 245, doi:10.2307/1907187.

Martin, R. V., D. J. Jacob, K. Chance, T. P. Kurosu, P. I. Palmer, and M. J. Evans (2003), Global inventory of nitrogen oxide emissions constrained by space-based observations of NO_2 columns, *J. Geophys. Res.*, *108*(D17), 4537, doi:10.1029/2003JD003453.

Martin, R. V., A. M. Fiore, and A. V. Donkelaar (2004), Space-based diagnosis of surface ozone sensitivity to anthropogenic emissions, *Geophys. Res. Lett.*, *31*, L06120, doi:10.1029/2004GL019416.

Meller, R., and G. K. Moortgat (2000), Temperature dependence of the absorption cross sections of formaldehyde between 223 and 323 K in the wavelength range 225–375 nm, *J. Geophys. Res.*, *105*, 7089–7101, doi:10.1029/1999JD901074.

Milford, J. B., A. G. Russell, and G. J. MCRAE (1989), A new approach to photochemical pollution-control: Implications of spatial patterns in pollutant responses to reductions in nitrogen-oxides and reactive organic gas emissions, *Environ. Sci. Technol.*, *23*(10), 1290–1301, doi:10.1021/es00068a017.

Millet, D. B., et al. (2006), Formaldehyde distribution over North America: Implications for satellite retrievals of formaldehyde columns and isoprene emission, *J. Geophys. Res.*, *111*, D24S02, doi:10.1029/2005JD006853.

Millet, D. B., D. J. Jacob, K. F. Boersma, T.-M. Fu, T. P. Kurosu, K. Chance, C. L. Heald, and A. Guenther (2008), Spatial distribution of isoprene emissions from North America derived from formaldehyde column measurements by the OMI satellite sensor, *J. Geophys. Res.*, *113*, D02307, doi:10.1029/2007JD008950.

Nagashima, T., T. Ohara, K. Sudo, and H. Akimoto (2010), The relative importance of various source regions on East Asian surface ozone, *Atmos. Chem. Phys.*, *10*(22), 11,305–11,322, doi:10.5194/acp-10-11305-2010.

Platt, U., and J. Stutz (2008), *Differential Optical Absorption Spectroscopy*, Springer Science & Business Media, Berlin.

Richter, A., J. P. Burrows, H. Nüß, C. Granier, and U. Niemeier (2005), Increase in tropospheric nitrogen dioxide over China observed from space, *Nature*, *437*(7055), 129–132, doi:10.1038/nature04092.

Saha, S., et al. (2010), The NCEP Climate Forecast System Reanalysis, *Bull. Am. Meteorol. Soc.*, *91*(8), 1015–1057, doi:10.1175/2010BAMS3001.1.

Schneider, U., A. Becker, P. Finger, A. Meyer-Christoffer, M. Ziese, and B. Rudolf (2013), GPCC's new land surface precipitation climatology based on quality-controlled in situ data and its role in quantifying the global water cycle, *Theor. Appl. Climatol.*, *115*(1–2), 15–40, doi:10.1007/s00704-013-0860-x.

Sen, P. K. (1968), Estimates of the regression coefficient based on Kendall's tau, *J. Am. Stat. Assoc.*, *63*(324), 1379–1389, doi:10.1080/01621459.1968.10480934.

Shao, M., Y. Zhang, L. Zeng, X. Tang, J. Zhang, L. Zhong, and B. Wang (2009), Ground-level ozone in the Pearl River Delta and the roles of VOC and NO, *J. Environ. Manage.*, *90*(1), 512–518, doi:10.1016/j.jenvman.2007.12.008.

Sillman, S. (1995), The use of NO_y, H_2O_2, and HNO_3 as indicators for ozone-NO_x -hydrocarbon sensitivity in urban locations, *J. Geophys. Res.*, *100*, 14,175–14,188, doi:10.1029/94JD02953.

Sillman, S., and F. J. Samson (1995), Impact of temperature on oxidant photochemistry in urban, polluted rural and remote environments, *J. Geophys. Res.*, *100*, 11,497–11,508, doi:10.1029/94JD02146.

Sillman, S. (2003), 9.11- Tropospheric Ozone and Photochemical Smog, in *Treatise on Geochemistry*, edited by H. D. Holland and K. K. Turekian, pp. 407–431, Pergamon, Oxford, doi:10.1016/B0-08-043751-6/09053-8.

Song, Y., M. Shao, Y. Liu, S. Lu, and W. Kuster (2007), Source apportionment of ambient volatile organic compounds in Beijing, *Environ. Sci. Technol.*, *41*, 4348–4353, doi:10.1021/es0625982.

Stavrakou, T., J. F. Müller, K. F. Boersma, R. J. van der A, J. Kurokawa, T. Ohara, and Q. Zhang (2013), Key chemical NO_x sink uncertainties and how they influence top-down emissions of nitrogen oxides, *Atmos. Chem. Phys.*, *13*(17), 9057–9082, doi:10.5194/acp-13-9057-2013.

Stavrakou, T., J. F. Müller, M. Bauwens, I. De Smedt, M. Van Roozendael, A. Guenther, M. Wild, and X. Xia (2014), Isoprene emissions over Asia 1979–2012: Impact of climate and land use changes, *Atmos. Chem. Phys.*, *14*(9), 4587–4605, doi:10.5194/acp-14-4587-2014.

Streets, D. G., et al. (2003), An inventory of gaseous and primary aerosol emissions in Asia in the year 2000, *J. Geophys. Res.*, *108*(D21), 8809, doi:10.1029/2002JD003093.

Tang, G., Y. Wang, X. Li, D. Ji, S. Hsu, and X. Gao (2012), Spatial-temporal variations in surface ozone in Northern China as observed during 2009–2010 and possible implications for future air quality control strategies, *Atmos. Chem. Phys.*, *12*(5), 2757–2776, doi:10.5194/acp-12-2757-2012.

van der A, R. J., D. H. M. U. Peters, H. Eskes, K. F. Boersma, M. Van Roozendael, I. De Smedt, and H. M. Kelder (2006), Detection of the trend and seasonal variation in tropospheric NO_2 over China, *J. Geophys. Res.*, *111*, D12317, doi:10.1029/2005JD006594.

Vrekoussis, M., F. Wittrock, A. Richter, and J. P. Burrows (2010), GOME-2 observations of oxygenated VOCs: What can we learn from the ratio glyoxal to formaldehyde on a global scale?, *Atmos. Chem. Phys.*, *10*(21), 10,145–10,160, doi:10.5194/acp-10-10145-2010.

Wang, H., C. S. Kiang, X. Tang, X. Zhou, and L. W. Chameides (2005), Surface ozone: A likely threat to crops in Yangtze delta of China, *Atmos. Environ.*, *39*, 3843–3850, doi:10.1016/j.atmosenv.2005.02.057.

Wang, H., Z. Lijun, and T. Xiaoyan (2006), Ozone concentrations in rural regions of the Yangtze Delta in China, *J. Atmos. Chem.*, *54*(3), 255–265, doi:10.1007/s10874-006-9024-z.

Wang, H., L. Fu, Y. Zhou, X. Du, and W. Ge (2010), Trends in vehicular emissions in China's mega cities from 1995 to 2005, *Environ. Pollut.*, *158*, 394–400, doi:10.1016/j.envpol.2009.09.002.

Wang, L. T., Z. Wei, J. Yang, Y. Zhang, F. F. Zhang, J. Su, C. C. Meng, and Q. Zhang (2014), The 2013 severe haze over southern Hebei, China: Model evaluation, source apportionment, and policy implications, *Atmos. Chem. Phys.*, *14*(6), 3151–3173, doi:10.5194/acp-14-3151-2014.

Wang, T., A. Ding, J. Gao, and W. S. Wu (2006), Strong ozone production in urban plumes from Beijing, China, *Geophys. Res. Lett.*, *33*, L21806, doi:10.1029/2006GL027689.

Wang, T., et al. (2010), Air quality during the 2008 Beijing Olympics: Secondary pollutants and regional impact, *Atmos. Chem. Phys.*, *10*(16), 7603–7615, doi:10.5194/acp-10-7603-2010.

Wang, Y., M. B. McElroy, J. W. Munger, J. Hao, H. Ma, C. P. Nielsen, and Y. Chen (2008), Variations of O_3 and CO in summertime at a rural site near Beijing, *Atmos. Chem. Phys.*, *8*, 6355–6363.

Wang, Y., Y. Zhang, J. Hao, and M. Luo (2011), Seasonal and spatial variability of surface ozone over China: Contributions from background and domestic pollution, *Atmos. Chem. Phys.*, *11*(7), 3511–3525, doi:10.5194/acp-11-3511-2011.

Wei, W., S. Wang, S. Chatani, Z. Klimont, J. Cofala, and J. Hao (2008), Emission and speciation of nonmethane volatile organic compounds from anthropogenic sources in China, *Atmos. Environ.*, *42*(20), 4976–4988, doi:10.1016/j.atmosenv.2008.02.044.

Wei, X. L., Y. S. Li, K. S. Lam, A. Y. Wang, and T. J. Wang (2007), Impact of biogenic VOC emissions on a tropical cyclone-related ozone episode in the Pearl River Delta region, China, *Atmos. Environ.*, *41*(36), 7851–7864, doi:10.1016/j.atmosenv.2007.06.012.

Wilks, D. S. (2011), *Statistical Methods in the Atmospheric Sciences*, Elsevier, Amsterdam.

Witte, J. C., M. R. Schoeberl, A. R. Douglass, J. F. Gleason, N. A. Krotkov, J. C. Gille, K. E. Pickering, and N. Livesey (2009), Satellite observations of changes in air quality during the 2008 Beijing Olympics and Paralympics, *Geophys. Res. Lett.*, *36*, L17803, doi:10.1029/2009GL039236.

Witte, J. C., B. N. Duncan, A. R. Douglass, and T. P. Kurosu (2011), The unique OMI $HCHO/NO_2$ feature during the 2008 Beijing Olympics: Implications for ozone production sensitivity, *Atmos. Environ.*, *45*(18), 3103–3111, doi:10.1016/j.atmosenv.2011.03.015.

Xing, J., S. X. Wang, C. Jang, Y. Zhu, and J. M. Hao (2011), Nonlinear response of ozone to precursor emission changes in China: A modeling study using response surface methodology, *Atmos. Chem. Phys.*, *11*(10), 5027–5044, doi:10.5194/acp-11-5027-2011.

Zhang, J., T. Wang, W. L. Chameides, C. Cardelino, J. Kwok, D. R. Blake, A. Ding, and K. L. So (2007), Ozone production and hydrocarbon reactivity in Hong Kong, Southern China, *Atmos. Chem. Phys.*, *7*, 557–573.

Zhang, Q., et al. (2007), NO_x emission trends for China, 1995–2004: The view from the ground and the view from space, *J. Geophys. Res.*, *112*, D22306, doi:10.1029/2007JD008684.

Zhang, Q., et al. (2009), Asian emissions in 2006 for the NASA INTEX-B mission, *Atmos. Chem. Phys.*, *9*(14), 5131–5153, doi:10.5194/acp-9-5131-2009.

Zhang, Q., B. Yuan, M. Shao, X. Wang, S. Lu, K. Lu, M. Wang, L. Chen, C. C. Chang, and S. C. Liu (2014), Variations of ground-level O_3 and its precursors in Beijing in summertime between 2005 and 2011, *Atmos. Chem. Phys.*, *14*(12), 6089–6101, doi:10.5194/acp-14-6089-2014.

Zhang, Y. H., et al. (2008), Regional ozone pollution and observation-based approach for analyzing ozone–precursor relationship during the PRIDE-PRD2004 campaign, *Atmos. Environ.*, *42*, 6203–6218, doi:10.1016/j.atmosenv.2008.05.002.

Zhao, B., S. X. Wang, H. Liu, J. Y. Xu, K. Fu, Z. Klimont, J. M. Hao, K. B. He, J. Cofala, and M. Amann (2013), NO_x emissions in China: Historical trends and future perspectives, *Atmos. Chem. Phys.*, *13*(19), 9869–9897, doi:10.5194/acp-13-9869-2013.

Zhao, C., Y. Wang, and T. Zeng (2009), East China Plains: A "basin" of ozone pollution, *Environ. Sci. Technol.*, *43*(6), 1911–1915, doi:10.1021/es8027764.

Zhao, Y., S. Wang, L. Duan, Y. Lei, P. Cao, and J. Hao (2008), Primary air pollutant emissions of coal-fired power plants in China: Current status and future prediction, *Atmos. Environ.*, *42*(36), 8442–8452, doi:10.1016/j.atmosenv.2008.08.021.

Zheng, J., M. Shao, W. Che, L. Zhang, L. Zhong, Y. Zhang, and D. Streets (2009), Speciated VOC emission inventory and spatial patterns of ozone formation potential in the Pearl River Delta, China, *Environ. Sci. Technol.*, *43*(22), 8580–8586, doi:10.1021/es901688e.

Zhihui, W. (2003), A biogenic volatile organic compounds emission inventory for Beijing, *Atmos. Environ.*, *37*(27), 3771–3782, doi:10.1016/S1352-2310(03)00462-X.